Two-Dimensional Cyclic Chaotic System for Noise-Reduced OFDM-DCSK Communication

Zhongyun Hua, *Senior Member, IEEE*, Zihua Wu, Yinxing Zhang, Han Bao, *Member, IEEE*, and Yicong Zhou, *Senior Member, IEEE*

***Abstract*— Secure communication techniques can protect data confidentiality during transmission through public channels. Chaotic systems are commonly used in secure communication due to their random-like behavior, unpredictability, and ergodicity. However, existing chaos-based secure communication schemes have some drawbacks concerning the chaotic systems used and the communication structures, so they cannot achieve satisfactory performance to resist transmission channel noise. In light of this, in this paper, we propose a two-dimensional (2D) cyclic chaotic system (2D-CCS) and design a novel chaos-based secure communication scheme called noise-reduced orthogonal frequency division multiplexing based differential chaos shift keying (NR-OFDM-DCSK). The 2D-CCS is a general framework that can generate a large number of new 2D chaotic maps using existing one-dimensional (1D) chaotic maps as seed maps. Theoretical analysis and experiment results demonstrate its robust chaotic behaviors. The NR-OFDM-DCSK employs a new chaotic map generated by 2D-CCS as the chaos generator, and its structure exhibits a strong ability to resist channel noise, as demonstrated by formulaic analysis. Our extensive experiments show that our developed 2D chaotic maps are more suitable for secure communication applications than existing 2D chaotic maps, and our NR-OFDM-DCSK can achieve a lower bit-error-rate (BER) than state-of-the-art secure communication schemes.**

***Index Terms*— Chaotic system, chaos-based practicality, secure communication, chaotic communication.**

Manuscript received 25 March 2024; revised 28 June 2024; accepted 26 August 2024. Date of publication 19 September 2024; date of current version 9 January 2025. This work was supported in part by the National Natural Science Foundation of China under Grant 62071142 and Grant 62201094, in part by Guangdong Basic and Applied Basic Research Foundation under Grant 2024A1515012299, in part by Guangdong Provincial Key Laboratory of Novel Security Intelligence Technologies under Grant 2022B1212010005, and in part by Shenzhen Science and Technology Program under Grant ZDSYS20210623091809029. This article was recommended by Associate Editor L. Gan. *(Corresponding author: Yinxing Zhang.)*

Zhongyun Hua is with the School of Computer Science and Technology, Harbin Institute of Technology, Shenzhen, Guangdong 518055, China, and also with Guangdong Provincial Key Laboratory of Novel Security Intelligence Technologies, Shenzhen 518055, China (e-mail: huazhongyun@hit.edu.cn).

Zihua Wu is with the School of Computer Science and Technology, Harbin Institute of Technology, Shenzhen, Guangdong 518055, China (e-mail: ozoa91011@gmail.com).

Yinxing Zhang is with the Faculty of Information Engineering and Automation, Kunming University of Science and Technology, Kunming 650500, China (e-mail: yxzhang23@163.com).

Han Bao is with the School of Microelectronics and Control Engineering, Changzhou University, Changzhou 213164, China (e-mail: charlesbao0319@gmail.com).

Yicong Zhou is with the Department of Computer and Information Science, University of Macau, Macau, China (e-mail: yicongzhou@um.edu.mo).

This article has supplementary downloadable material available at https://doi.org/10.1109/TCSI.2024.3454535, provided by the authors.

Digital Object Identifier 10.1109/TCSI.2024.3454535

I. Introduction

SECURE communication refers to the exchange of information or data between parties in a manner that ensures confidentiality [1]. The phenomenon of the butterfly effect, or chaotic behavior, was first observed in natural occurrences [2]. Due to the random-like behavior, initial state sensitivity, and parameter controllability [3], [4], chaotic systems are commonly employed in diverse applications like secure communication [5], [6], time series prediction [7], pseudo-random number generators [8], and image encryption [9]. When used for secure communications, chaotic systems provide benefits such as high transmission rate, high security, and low bit-error-rate (BER). Consequently, it has become customary to develop secure communication schemes using chaotic systems.

Since the early 1990s, chaotic system has been utilized for developing secure communication schemes [10]. Up to now, numerous chaos-based secure communication schemes have been developed [11] and can be classified into two categories based on the way they modulate the transmitted data: coherent chaotic communication and non-coherent chaotic communication [12]. The non-coherent chaotic communication is considered more practical since it does not require a chaotic synchronizer [13]. As a typical example of non-coherent chaotic communication, the differential chaos shift keying (DCSK) [14] transmits a reference sequence and an information-bearing sequence during one DCSK symbol duration. Due to its many unique properties, such as simple circuit structure and fixed threshold decision component, DCSK exhibits practical advantages. However, the traditional DCSK structure requires a delay line, which causes extra complexity and difficulty in actual circuit implementation. Furthermore, it cannot achieve a high data transmission rate and satisfactory noise resistance ability because half of the transmitted data is used for delivering the reference signal, and the receiver can not separate the channel noise from the transmitted signal during demodulation.

Recently, a multitude of modified DCSKs [15], [16], [17] have been developed to overcome the drawbacks of the original design. For example, Li et al. [15] devised an orthogonal frequency division multiplexing based DCSK (OFDM-DCSK) that is able to transmit multiple information bits simultaneously using the efficient exploitation of frequency bands. Additionally, OFDM-DCSK eliminates the need for a delay line. On this basis, Liu et al. [16] put forth a frequency-and-time hybrid-interleaving OFDM-based

DCSK (FH-OFDM-DCSK), which enhances the security of OFDM-DCSK by utilizing the frequency diversity brought by frequency hopping. Chen et al. [17] proposed an OFDM-based pre-coded chaos shift keying (OFDM-PC-CSK) communication scheme, which does not need to transmit the reference signal and thus improves the data transmission efficiency compared with OFDM-DCSK.

For these chaos-based DCSKs, their performance is determined not only by their communication structure but also by the chaotic system they employ. Many novel chaotic systems [18], [19], [20], [21], [22] with complex dynamics behaviors have recently been developed using various techniques. However, most of existing chaotic systems perform poorly in secure communication applications for the following reasons. Firstly, their chaotic intervals are discontinuous [23]. Since all digital platforms have finite precision, the digitized parameters of chaotic systems can only be approximated when implemented on digital platforms. If the chaotic intervals are discontinuous, a slight perturbation to the parameters may cause the parameters to be out of the chaotic intervals, leading the chaotic behavior to degenerate into periodic behavior. Secondly, the chaotic sequences they produce are non-uniformly distributed and have a low degree of randomness [24], which can negatively impact the performance of secure communication in terms of BER and security since the generated chaotic sequences are used to modulate transmission data.

Existing communication schemes also have certain limitations in resisting transmission noise and ensuring security. When signals are transmitted through noisy channels, they may be blurred by the channel noise. Many previous communication schemes demodulate the channel noise along with the original signal at the receiver, treating it as part of the signal, and causing a relatively high BER [25]. Moreover, these schemes often send information in a relatively straightforward way, making it defenseless to being eavesdropped by malicious third parties. For example, OFDM-DCSK [15] modulates multiple information bits using the same chaotic sequence within a given time period, creating obvious patterns in the transmitted signals across different frequency bands. Therefore, it is crucial to develop communication schemes with strong noise resistance ability and high security.

In light of the above, in this paper, we aim to study a new secure communication scheme to overcome the shortcomings of existing schemes. At first, we propose the two-dimensional (2D) cyclic chaotic system (2D-CCS), a general framework for producing new 2D chaotic maps by using existing one-dimensional (1D) chaotic maps as seed maps. High-dimensional (HD) chaotic systems are well-suited for secure communication due to their ability to exhibit hyperchaotic behaviors and complex dynamical properties [26], [27]. However, implementing these HD systems requires substantial computational resources because of their complexity and numerous variables. Generally, a chaotic system with high dimensions has a more complex structure and requires more implementation resources. 1D chaotic maps lack hyperchaotic behavior and thus offer relatively low security when applied in secure communication. This is because these trajectories may be predicted using some artificial intelligence techniques [28], [29]. Once the trajectory of a chaotic map has been accurately predicted, the map loses its unpredictability, which can lead to the failure of the communication scheme. A chaotic system's behavior is much more difficult to predict if it has hyperchaotic behavior [21], [30]. As for 2D chaotic maps, they can possess hyperchaotic behavior and balance system implementation costs and security, compromising between 1D and HD chaotic systems. Theoretical analysis and experimental results prove its continuous chaotic interval and robust chaotic behavior. Three new 2D chaotic maps generated by 2D-CSS are taken as examples to demonstrate the effectiveness of 2D-CCS. Performance analysis demonstrates that the three new 2D chaotic maps have continuous chaotic intervals uniformly distributed outputs, and a high degree of randomness.

Taking one new 2D chaotic map as the chaos generator, we further design a novel chaos-based secure communication scheme, namely noise-reduced OFDM-DCSK (NR-OFDM-DCSK). At the transmitter, the information bits are modulated using a chaotic modulation module, a scrambling module, and an IFFT module to get the transmitted signal. At the receiver, the received signals are demodulated using an FFT module, a descrambling module, an averaging filter module, and a chaotic demodulation module to extract the information bits. Theoretical analysis shows that NR-OFDM-DCSK has great noise resistance ability. Experimental results demonstrate that our new chaotic maps can achieve better performance than existing chaotic maps in secure communication applications, and our NR-OFDM-DCSK has better noise resistance ability than state-of-the-art DCSKs when using the same chaotic map as the chaos generator.

We summarize our contributions as follows.

1) We propose 2D-CCS as a general framework that can generate a large number of new 2D chaotic maps using existing 1D chaotic maps as seed maps. Formulaic analysis proves the hyperchaotic behavior of 2D-CCS in the sense of the Lyapunov exponent (LE).
2) We generate three new 2D chaotic maps as examples using 2D-CCS. Experimental results show that the new 2D chaotic maps exhibit favorable chaos properties and better performance indicators in contrast to existing 2D chaotic maps.
3) We develop a new secure communication scheme NR-OFDM-DCSK. Formulaic analysis shows its low BER over the additive white Gaussian noise (AWGN) channel.
4) Experimental results show that our new chaotic maps are more suitable for secure communication applications than existing 2D chaotic maps, and our NR-OFDM-DCSK exhibits better noise resistance ability than state-of-the-art secure communication schemes.

The rest of this paper is organized as follows. Section II introduces 2D-CCS and theoretically proves its hyperchaotic behavior. Section III provides three new 2D chaotic maps generated by 2D-CCS as examples and evaluates their performance. Section IV introduces NR-OFDM-DCSK and analyzes its theoretical BER over the AWGN channel. Section V evaluates the performance of NR-OFDM-DCSK from various aspects, and Section VI concludes this paper.

II. 2D-CCS

This section presents the details of 2D-CCS and then proves its hyperchaotic behaviors in the sense of LE.

A. Construction of 2D-CCS

2D-CCS is constructed from an existing 1D seed chaotic map with two linear expressions. The output of each dimension of 2D-CCS is obtained by first combining the seed map with a linear expression, and then applying a modulo operation to the combined result to confine the phase space of the system within a bounded space. Therefore, the mathematical definition of 2D-CCS is given as

$$\begin{cases} x_1(i+1) = p_1 x_1(i) + F(x_2(i)) \mod M \\ x_2(i+1) = F(x_1(i)) + p_2 x_2(i) \mod M, \end{cases} \tag{1}$$

where $\mathbf{x}(i) = [x_1(i), x_2(i)]^T$ is the state vector of 2D-CCS at the i-th observation time, p_1 and p_2 are two control parameters, $F(\cdot)$ is the 1D seed map chosen by the system constructor, and M is the modular coefficient. As can be seen in Eq. (1), the seed map and two linear expressions form a cyclic shift relationship between the two dimensions.

To achieve robust hyperchaotic behavior, the control parameters of 2D-CCS should satisfy a specific condition, which will be theoretically derived in the following section. As the condition is particularly relevant to the construction of 2D-CCS, we present it here as follows:

$$|p_k| > \max_{x\in[0,M)} (|f(x)|) + 1, \tag{2}$$

where $k \in \{1, 2\}$ and $f(x)$ is the derivative of the seed $F(x)$. The above condition requires that the seed $F(x)$ must be differentiable, and its absolute derivative $|f(x)|$ must have a maximum value within $x \in [0, M)$. To the best of our knowledge, most existing 1D chaotic maps share this property, such as the fraction map, logistic map, and sine map.

B. Existence of Hyperchaos

This subsection explains how to derive Eq. (2) from a mathematical standpoint.

1) Preliminaries: The LE indicator is one of the most commonly used methods to prove the existence of chaos [31]. It measures the divergence rate of a dynamic system's two trajectories that begin with close initial states. A larger LE indicates a faster divergence of two trajectories, which further implies a more complex dynamics behavior of a dynamic system [32]. For a 2D dynamic system, two LEs can be computed. Therefore, we present the definition of chaos in the sense of LE in Definition 1 [33].

Definition 1 [33]: A dynamic system has chaotic behavior in the sense of LE if: 1) its phase space is globally bounded; 2) it has at least one positive LE. Besides, a dynamic system with globally bounded phase space has hyperchaotic behavior if it has more than one positive LEs.

Furthermore, two theorems are introduced as background. Theorem 1 concerns the Geršgorin-type inclusion set of matrix singular values, while Theorem 2 relates to the singular value characteristics of matrix products.

Theorem 1 [34]: For a square matrix $\mathbf{A} = (a_{ij}) \in \mathbb{C}^{n\times n}$, denote the sum of the absolute values of its off-diagonal elements at row k and column k as $r_k = \sum_{j=1, j\neq k}^{n} |a_{kj}|$ and $c_k = \sum_{i=1, i\neq k}^{n} |a_{ik}|$, respectively. Then all n singular values of the matrix fall within the interval $C(\mathbf{A}) := \bigcup_{k=1}^{n} C_k$, where $C_k = \left[\max\{0, |a_{kk}| - s_k\}, |a_{kk}| + s_k\right]$, and $s_k = \max\{r_k, c_k\}$.

Theorem 2 [35]: (The singular values in this theorem are arranged in descending order, i.e., $\sigma_1 \geq \sigma_2 \geq \cdots \geq \sigma_n$.) Any two matrices $\mathbf{A}, \mathbf{B} \in \mathbb{C}^{n\times n}$ satisfy that $\sigma_k(\mathbf{AB}) \geq \max\{\sigma_k(\mathbf{A})\sigma_n(\mathbf{B}), \sigma_k(\mathbf{B})\sigma_n(\mathbf{A})\}$ for $k \in \{1, 2, \ldots, n\}$.

2) Proof of Hyperchaos: For a 2D dynamic system, its two LEs can be calculated as [36]

$$LE_k = \lim_{t\to\infty} \frac{1}{t} \ln\left(\lambda_k(\mathbf{J}_t)\right), \tag{3}$$

where $\lambda_k(\mathbf{J}_t)$ is the k-th eigenvalue of $\mathbf{J}_t = \prod_{i=0}^{t-1} \mathbf{J}_{\mathbf{x}(i)}$, $k \in \{1, 2\}$, and $\mathbf{J}_{\mathbf{x}(i)}$ is the Jacobian matrix of the 2D dynamic system with the observed state $\mathbf{x}(i)$. Specifically, the Jacobian matrix of 2D-CCS with the observed state $\mathbf{x}(i)$ is defined as

$$\mathbf{J}_{\mathbf{x}(i)} = \begin{pmatrix} \frac{\partial x_1(i+1)}{\partial x_1(i)}|_{\mathbf{x}(i)} & \frac{\partial x_1(i+1)}{\partial x_2(i)}|_{\mathbf{x}(i)} \\ \frac{\partial x_2(i+1)}{\partial x_1(i)}|_{\mathbf{x}(i)} & \frac{\partial x_2(i+1)}{\partial x_2(i)}|_{\mathbf{x}(i)} \end{pmatrix} = \begin{pmatrix} p_1 & f(x_2(i)) \\ f(x_1(i)) & p_2 \end{pmatrix}. \tag{4}$$

Based on the strong correlation between a matrix's eigenvalues and its singular values, we can convert the computation of eigenvalues in Eq. (3) into that of singular values. To elucidate the properties of $\mathbf{J}_t$'s singular values, we introduce Lemma 1 as follows.

Lemma 1: When Eq. (2) holds, the two singular values of $\mathbf{J}_t$ are both greater than one.

Proof: According to Theorem 1, the two singular values of $\mathbf{J}_{\mathbf{x}(i)}$ will fall within the interval $C(\mathbf{J}_{\mathbf{x}(i)}) := \bigcup_{k=1}^{2} C_k$, where $C_k = \left[\max\{0, |p_k| - s_k\}, |p_k| + s_k\right]$, $s_k = \max\{r_k, c_k\}$, $r_k = |f(x_{3-k}(i))|$, and $c_k = |f(x_k(i))|$. Since s_k is essentially a value of $|f(x)|$ for $x \in [0, M)$, we can derive that

$$s_k \leq \max_{x\in[0,M)} (|f(x)|). \tag{5}$$

When Eq. (2) holds, we can further derive that

$$|p_k| - s_k > \max_{x\in[0,M)} (|f(x)|) + 1 - s_k \geq 1, \tag{6}$$

and

$$\max\{0, |p_k| - s_k\} = |p_k| - s_k > 1. \tag{7}$$

On this basis, the lower bound of C_k is greater than 1, meaning that the two singular values of $\mathbf{J}_{\mathbf{x}(i)}$ within $C(\mathbf{J}_{\mathbf{x}(i)})$ are also greater than one. Therefore, the two singular values of $\mathbf{J}_{\mathbf{x}(i)}$ can be denoted as

$$\sigma_1(\mathbf{J}_{\mathbf{x}(i)}) \geq \sigma_2(\mathbf{J}_{\mathbf{x}(i)}) > 1. \tag{8}$$

Since $\mathbf{J}_t$ is the matrix product of $\mathbf{J}_{\mathbf{x}(i)}$ at each observation time in $\{0, 1, \ldots, t-1\}$, the two singular values of $\mathbf{J}_t$, denoted as $\sigma_1(\mathbf{J}_t) \geq \sigma_2(\mathbf{J}_t)$, satisfy the following equation according to Theorem 2 and Eq. (8):

$$\begin{aligned} \sigma_1(\mathbf{J}_t) \geq \sigma_2(\mathbf{J}_t) &= \sigma_2(\mathbf{J}_{t-1}\mathbf{J}_{\mathbf{x}(t-1)}) \\ &\geq \sigma_2(\mathbf{J}_{t-1})\sigma_2(\mathbf{J}_{\mathbf{x}(t-1)}) \\ &\geq \sigma_2(\mathbf{J}_{\mathbf{x}(0)})\sigma_2(\mathbf{J}_{\mathbf{x}(1)}) \cdots \sigma_2(\mathbf{J}_{\mathbf{x}(t-1)}) \\ &> 1. \end{aligned} \tag{9}$$

Thus, we have $\sigma_1(\mathbf{J}_t) \geq \sigma_2(\mathbf{J}_t) > 1$, which completes the proof of Lemma 1. ■

Based on Lemma 1, we introduce Proposition 1 to state that our 2D-CCS can exhibit hyperchaotic behavior.

Proposition 1: When Eq. (2) holds, the 2D-CCS described by Eq. (1) can exhibit hyperchaotic behavior.

Proof: From the knowledge of linear algebra and matrix analysis, the n eigenvalues $\lambda_1 \geq \lambda_2 \geq \cdots \geq \lambda_n$ and n singular values $\sigma_1 \geq \sigma_2 \geq \cdots \geq \sigma_n$ of an n order matrix satisfy that

$$\sigma_1 \geq |\lambda_k| \geq \sigma_n \tag{10}$$

for $k \in \{1, 2, \ldots, n\}$. According to Lemma 1, the two singular values of $\mathbf{J}_t$ satisfy that $\sigma_1(\mathbf{J}_t) \geq \sigma_2(\mathbf{J}_t) > 1$ when Eq. (2) holds. Based on this, the eigenvalues of $\mathbf{J}_t$ satisfy that

$$\left|\lambda_k(\mathbf{J}_t)\right| \geq \sigma_2(\mathbf{J}_t) > 1 \tag{11}$$

for $k \in \{1, 2\}$. Therefore, we can deduce from Eq. (3) that the LEs of 2D-CCS are positive, namely

$$LE_k \geq \lim_{t\to\infty} \frac{1}{t} \ln\left(\sigma_2(\mathbf{J}_t)\right) > 0, \tag{12}$$

where $k \in \{1, 2\}$. Based on the discussion above, 2D-CCS has two positive LEs when Eq. (2) holds, which meets the second condition of Definition 1.

On the other hand, as the output of each dimension of 2D-CCS is performed by modulo M, the phase space of 2D-CCS is globally bounded within $[0, M) \times [0, M)$, which fulfills the first condition of Definition 1. As the two conditions of Definition 1 are satisfied and 2D-CCS has more than one positive LE, the 2D-CCS shows hyperchaotic behavior in the sense of LE. This completes the proof of Proposition 1. ■

It is worth noting that if Eq. (2) is not satisfied, 2D-CCS may display periodic or unstable behavior. Therefore, to enable 2D-CCS to exhibit continuous and widespread chaotic intervals, we should ensure that the control parameters of 2D-CCS conform to Eq. (2). In addition, as the two singular values of $\mathbf{J}_{\mathbf{x}(i)}$ lie within the interval $C(\mathbf{J}_{\mathbf{x}(i)})$, which is associated with p_1 and p_2 according to Lemma 1, setting the absolute of p_1 and p_2 as larger values results in the positive interval $C(\mathbf{J}_{\mathbf{x}(i)})$ being farther from the origin, thus leading to larger singular values of $\mathbf{J}_{\mathbf{x}(i)}$. From Eq. (9), $\mathbf{J}_t$ has larger singular values as $\mathbf{J}_{\mathbf{x}(i)}$'s singular values increase. From Eqs. (11) and (12), the larger singular values of $\mathbf{J}_t$ enable its larger eigenvalues and thus result in larger LEs. Therefore, 2D-CCS can achieve larger LEs and show more complex dynamics behavior by setting its control parameters p_1 and p_2 as larger values. We will experimentally verify this in Section III-C.1.

III. Three Examples and Performance Evaluation

This section constructs three new 2D chaotic maps using 2D-CCS, analyzes their chaos properties, and compares them to other existing 2D chaotic maps.

A. Three New 2D Chaotic Maps

Based on Eq. (1), we employ the fraction map [37], logistic map [38], and sine map [39] as seed maps to construct the 2D fraction cyclic chaotic map (2D-FCCM), 2D logistic cyclic chaotic map (2D-LCCM), and 2D sine cyclic chaotic map (2D-SCCM), respectively. Notably, the modular coefficient M is set to 1 for simplicity, but it can be assigned other values without impacting the chaotic behavior of the chaotic maps generated by 2D-CCS, as long as their control parameters satisfy Eq. (2).

1) 2D-FCCM: 2D-FCCM is seeded by the fraction map with a parameter $a \in [0, 1]$ [37]. For simplicity, we have set $a = 1$ for the construction of 2D-FCCM. However, a can be assigned other values, which may result in a different range of values for the control parameters of 2D-FCCM according to Eq. (2). Specifically, the definitions of the fraction map and the constructed 2D-FCCM are

$$x(i+1) = \mathcal{F}(x(i)) = \frac{1}{x(i)^2 + 0.1} - ax(i), \tag{13}$$

and

$$\begin{cases} x_1(i+1) = p_1 x_1(i) + \dfrac{1}{x_2(i)^2 + 0.1} - x_2(i) & \mod 1 \\ x_2(i+1) = \dfrac{1}{x_1(i)^2 + 0.1} - x_1(i) + p_2 x_2(i) & \mod 1. \end{cases} \tag{14}$$

It is evident that the fraction map $\mathcal{F}(x(i))$ is differentiable, and its absolute derivative attains a maximum value of 21.5396 when $a = 1$ and $x(i) \in [0, 1)$. Thus, when $|p_k| > 22.5396$ for $k \in \{1, 2\}$, the condition specified in Eq. (2) holds, and 2D-FCCM can show hyperchaotic behavior as per Proposition 1.

2) 2D-LCCM: 2D-LCCM is seeded by the logistic map with a parameter $b \in [0, 4]$ [38]. For simplicity, we have set $b = 4$ in constructing 2D-LCCM. Nevertheless, b can take other values as well. The definitions of logistic map and the constructed 2D-LCCM are defined as follows:

$$x(i+1) = \mathcal{L}(x(i)) = bx(i)(1 - x(i)), \tag{15}$$

and

$$\begin{cases} x_1(i+1) = p_1 x_1(i) + 4x_2(i)(1 - x_2(i)) & \mod 1 \\ x_2(i+1) = 4x_1(i)(1 - x_1(i)) + p_2 x_2(i) & \mod 1. \end{cases} \tag{16}$$

The logistic map $\mathcal{L}(x(i))$ is differentiable, and its absolute derivative has a maximum value of 4 when $b = 4$ and $x(i) \in [0, 1)$. As a result, when $|p_k| > 5$ for $k \in \{1, 2\}$, Eq. (2) is satisfied and 2D-LCCM can show hyperchaotic behavior according to Proposition 1.

3) 2D-SCCM: 2D-SCCM is seeded by the sine map with a parameter $c \in [0, 1]$ [39]. For simplicity, we have set $c = 1$ for the construction of 2D-SCCM. Here are the definitions of the sine map and the constructed 2D-SCCM:

$$x(i+1) = \mathcal{S}(x(i)) = c \sin(\pi x(i)), \tag{17}$$

and

$$\begin{cases} x_1(i+1) = p_1 x_1(i) + \sin(\pi x_2(i)) & \mod 1 \\ x_2(i+1) = \sin(\pi x_1(i)) + p_2 x_2(i) & \mod 1. \end{cases} \tag{18}$$

The sine map $\mathcal{S}(x(i))$ is differentiable, and its absolute derivative attains a maximum value of π when $c = 1$ and $x(i) \in [0, 1)$. Therefore, when $|p_k| > \pi + 1$ for $k \in \{1, 2\}$, Eq. (2) holds and 2D-SCCM can show hyperchaotic behavior according to Proposition 1.

Based on the examples above, we can observe that by selecting different seed maps and parameter settings, 2D-CCS can generate numerous new 2D chaotic maps. It is worth noting that when the parameters $p_1 = p_2$ and the initial values $x_1(0) = x_2(0)$, the 2D chaotic map can degenerate into a 1D chaotic map. However, we can easily avoid this situation by selecting distinct control parameters and initial values.

TABLE I
THE FIXED POINTS OF 2D-FCCM, 2D-LCCM, AND 2D-SCCM, AND THE ABSOLUTE EIGENVALUES OF THEIR JACOBIAN MATRICES AT EACH FIXED POINT

Chaotic maps	Parameters (p_1, p_2)	Fixed points $(\tilde{x}_1, \tilde{x}_2)$	Absolute eigenvalues $(\lvert\lambda_1\rvert, \lvert\lambda_2\rvert)$
2D-FCCM	$(23, 23)$	$(0,0), (0.7350, 0.3715), (0.3715, 0.7350)$	$(22, 24), (31.0461, 14.9539), (31.0461, 14.9539)$
	$(-24, 25)$	$(0, 0)$	$(24.0204, 25.0204)$
2D-LCCM	$(6, 6)$	$(0,0), (0.2500, 0.2500), (0.6096, 0.6096)$	$(2, 10), (4, 8), (5.1232, 6.8768)$
	$(-7, 8)$	$(0,0), (0.5000, 0)$	$(8, 9), (7, 8)$
2D-SCCM	$(5, 5)$	$(0,0), (0.5000, 0), (0.5000, 0.5000), (0, 0.5000)$	$(1.8584, 8.1416), (5, 5), (5, 5), (5, 5)$
	$(-6, 7)$	$(0,0), (0.2344, 0.2214), (0, 0.5000)$	$(6.7194, 7.7194), (6.4184, 7.4184), (6, 7)$

B. Chaos Properties Analysis

1) Fixed-Point Stability: A fixed point of a function is the point that maps to itself by the function. For example, the fixed points of 2D-FCCM, 2D-LCCM, and 2D-SCCM, denoted as $(\tilde{x}_1, \tilde{x}_2)$, are the solutions of the following equations:

$$\begin{cases} \tilde{x}_1 = p_1\tilde{x}_1 + \dfrac{1}{\tilde{x}_2^2 + 0.1} - \tilde{x}_2 \mod 1 \\ \tilde{x}_2 = \dfrac{1}{\tilde{x}_1^2 + 0.1} - \tilde{x}_1 + p_2\tilde{x}_2 \mod 1, \end{cases} \tag{19a}$$

$$\begin{cases} \tilde{x}_1 = p_1\tilde{x}_1 + 4\tilde{x}_2(1 - \tilde{x}_2) \mod 1 \\ \tilde{x}_2 = 4\tilde{x}_1(1 - \tilde{x}_1) + p_2\tilde{x}_2 \mod 1, \end{cases} \tag{19b}$$

$$\begin{cases} \tilde{x}_1 = p_1\tilde{x}_1 + \sin(\pi\tilde{x}_2) \mod 1 \\ \tilde{x}_2 = \sin(\pi\tilde{x}_1) + p_2\tilde{x}_2 \mod 1. \end{cases} \tag{19c}$$

A fixed point may be stable or unstable, depending on whether nearby states are attracted to or rejected by the fixed point. The stability of a fixed point can be represented by the system's gradient at that point. For a 2D dynamic system, its two gradients at a point, denoted as λ_1 and λ_2, are the two eigenvalues of its Jacobian matrix at the point. If $|\lambda_1| > 1$ and $|\lambda_2| > 1$, the fixed point is unstable and the system keeps oscillating. Otherwise, the fixed point is stable and the system remains steady as it evolves.

For different parameter pairs (p_1, p_2), Table I lists the fixed points of the three chaotic maps and the absolute eigenvalues of their Jacobian matrices at each fixed point. It can be seen that the chaotic maps have different numbers of fixed points under different parameters. Besides, all absolute eigenvalues are greater than 1, meaning that every fixed point is unstable, and these chaotic maps keep oscillating as they evolve.

2) Ability to Delay Chaos Degradation: Due to limited digital precision, all chaotic maps implemented on digital platforms eventually degenerate into periodic behaviors, a phenomenon known as chaos degradation. Chaotic maps that exhibit later chaos degradation times are more suitable for practical applications. However, as it is difficult to directly measure the chaos degradation time of a chaotic map, previous works have tested this ability by examining the randomness of the generated chaotic sequence. A chaotic map is considered to have a high ability to delay chaos degradation if its generated sequence passes a strict randomness test. A failed test indicates that the chaotic behavior has degenerated into periodic behavior within the length of the tested sequence.

TestU01 [40] is considered to be a very stringent standard for randomness testing and can test longer random sequences than other standards. It consists of eight test batteries: Rabbit, Alphabit, BlockAlphabit, SmallCrush, Crush, BigCrush, pseudoDIEHARD, and FIPS-140-2. The Rabbit, Alphabit, and BlockAlphabit batteries allow user-specified test data sizes, while the other batteries utilize default test data sizes. Each test battery contains a varying number of sub-tests, and each sub-test yields a p-value. A given random sequence passes a sub-test if its p-value falls within the range of $[0.001, 0.999]$.

TABLE II
PARAMETER SETTINGS AND INITIAL STATES OF 2D-FCCM, 2D-LCCM, AND 2D-SCCM IN THE TESTU01 TEST, TRAJECTORY, CD, AND IE EXPERIMENTS

Chaotic maps	Parameter settings	Initial states
2D-FCCM	$(p_1, p_2) = (40, 34)$	$(0.0971, 0.8235)$
2D-LCCM	$(p_1, p_2) = (93, 59)$	$(0.9619, 0.0046)$
2D-SCCM	$(p_1, p_2) = (48, 15)$	$(0.4411, 0.1970)$

TABLE III
TESTU01 TEST RESULTS FOR 2D-FCCM, 2D-LCCM, AND 2D-SCCM

Test battery	Data size	2D-FCCM	2D-LCCM	2D-SCCM
Rabbit	1 Gb	40/40	40/40	40/40
Alphabit	1 Gb	17/17	17/17	17/17
BlockAlphabit	1 Gb	102/102	102/102	102/102
SmallCrush	$\approx$ 6 Gb	15/15	15/15	15/15
Crush	$\approx$ 1 Tb	144/144	144/144	144/144
BigCrush	$\approx$ 10 Tb	160/160	160/160	160/160
pseudoDIEHARD	$\approx$ 5 Gb	126/126	126/126	126/126
FIPS-140-2	$\approx$ 19 Kb	16/16	16/16	16/16

The first-dimensional outputs of 2D-FCCM, 2D-LCCM, and 2D-SCCM are subject to TestU01 testing, whereby the test sequence is formed by extracting 8 bits from each output. The parameter pairs and initial states used in the three new chaotic maps are randomly selected, with their values specified in Table II. Table III lists the TestU01 test results, demonstrating that the three new chaotic maps can successfully pass all the test batteries in the TestU01 standard, and thus these chaotic maps have a high ability to delay chaos degradation.

C. Performance Comparison

This subsection presents a comparative analysis of our 2D-FCCM, 2D-LCCM, and 2D-SCCM with Bao's [41], Huang's [42], and Kong's [43] 2D chaotic maps from four perspectives: LE, trajectory, correlation dimension (CD), and information entropy (IE). For each chaotic map, a parameter range is required to calculate the LEs, while a fixed parameter value is used to calculate other indicators.

To provide a fair comparison, we set the parameters of our chaotic maps as small as possible that can make them show hyperchaotic behaviors. As a result, when calculating the LEs, the parameter ranges of our 2D-FCCM, 2D-LCCM, and 2D-SCCM are set as $p_1, p_2 \in [23, 122]$, $p_1, p_2 \in$

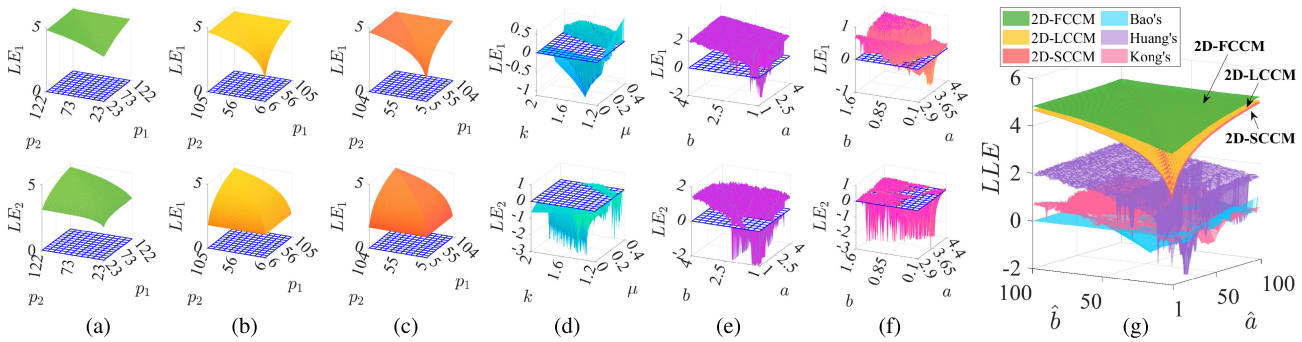

Fig. 1. The two LEs of (a) 2D-FCCM with parameters $p_1, p_2 \in [23, 122]$, (b) 2D-LCCM with parameters $p_1, p_2 \in [6, 105]$, (c) 2D-SCCM with parameters $p_1, p_2 \in [5, 104]$, (d) Bao's 2D chaotic map with parameters $\mu \in [0, 0.4], k \in [1.2, 2], a = -1, b = 1$, (e) Huang's 2D chaotic map with parameters $a, b \in [1, 4]$, (f) Kong's 2D chaotic map with parameters $a \in [2.9, 4.4], b \in [0.1, 1.6], c = d = 0$, and (g) LLE of different 2D chaotic maps with their control parameters scaled to $[1, 100]$.

TABLE IV

PARAMETER SETTINGS AND INITIAL STATES OF BAO'S, HUANG'S, AND KONG'S 2D CHAOTIC MAPS IN TRAJECTORY, CD, AND IE EXPERIMENTS

Chaotic maps	Parameter settings	Initial states
Bao's [41]	$(\mu, k, a, b) = (0.1, 1.88, -1, 1)$	$(0.5, 0.5)$
Huang's [42]	$(a, b) = (1.5, 2.9)$	$(0.5, 0.5)$
Kong's [43]	$(a, b, c, d) = (3.565, 0.4, 0, 0)$	$(1, -2)$

$[6, 105]$, and $p_1, p_2 \in [5, 104]$, respectively, because they show hyperchaotic behaviors when their parameters separately satisfy that $|p_k| > 22.5396$, $|p_k| > 5$, and $|p_k| > \pi + 1$ ($k \in \{1, 2\}$), according to the discussions in Section III-A. When calculating other indicators, their parameters are set as the randomly selected values shown in Table II to keep consistent with the previous experiments. The initial states of our chaotic maps used in all indicators also follow the values listed in Table II.

For Bao's [41], Huang's [42], and Kong's [43] 2D chaotic maps, we directly use the representative parameters and initial states presented in their original papers. Specifically, when calculating the LEs, the parameter ranges are set as $\mu \in [0, 0.4]$, $k \in [1.2, 2]$, $a = -1$, $b = 1$ in Bao's map [41], $a, b \in [1, 4]$ in Huang's map [42], and $a \in [2.9, 4.4]$, $b \in [0.1, 1.6]$, $c = d = 0$ in Kong's map [43], whereas their specified parameters for calculating other indicators and the initial states used in all indicators are listed in Table IV.

1) LE: As mentioned in Definition 1, a globally bounded dynamic system shows chaotic behavior with a positive LE and hyperchaotic behavior with multiple positive LEs. The larger the LE, the more complex the manifested chaotic behavior.

Fig. 1(a)-(c) display the two LEs of 2D-FCCM, 2D-LCCM, and 2D-SCCM, while Fig. 1(d)-(f) display the two LEs of Bao's, Huang's, and Kong's 2D chaotic maps. As can be seen, the two LEs of our new chaotic maps are positive over the entire parameter space, implying that they have continuous chaotic intervals and hyperchaotic behaviors. Nonetheless, the competing chaotic maps possess chaotic behaviors and positive LEs only within a restricted parameter space, meaning that their chaotic intervals are discontinuous. It can also be seen that the larger the parameters p_1 and p_2, the larger the LEs of our chaotic maps, validating the last paragraph of Section II-B. Fig. 1(g) plots each chaotic map's largest LE (LLE) to provide a more straightforward comparison. We replace their control parameters with $\hat{a}$ and $\hat{b}$ and scale them to within $[1, 100]$ for unification. As can be seen, the LLEs of our chaotic maps are much larger than those of the comparative chaotic maps.

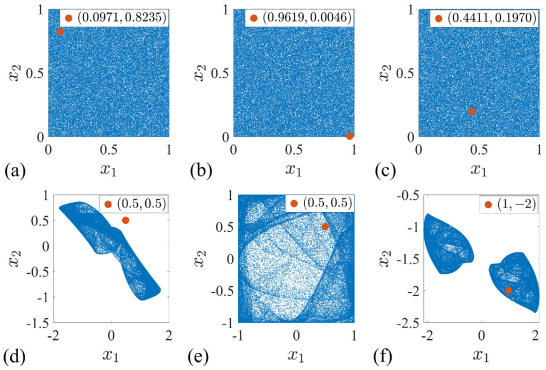

Fig. 2. Trajectories of (a) 2D-FCCM, (b) 2D-LCCM, (c) 2D-SCCM, (d) Bao's 2D chaotic map, (e) Huang's 2D chaotic map, and (f) Kong's 2D chaotic map.

2) Trajectory: The trajectory of a chaotic map provides a visual representation of how its outputs occupy the phase space. A chaotic map with a more uniform trajectory occupies a larger portion of the phase space. Fig. 2 depicts the trajectories of our 2D chaotic maps, as well as those of Bao, Huang, and Kong. Each trajectory contains 100,000 iteratively generated points, with the initial state marked by a red dot. As can be seen, the trajectories of our chaotic maps are uniformly distributed throughout their entire phase space, while those of the comparative chaotic maps only occupy a subset of their respective phase spaces. This suggests that the outputs of our chaotic maps are more uniform and less predictable.

3) CD: CD is a kind of fractal dimension that quantifies the space dimensionality occupied by a time series [44]. It is often used to verify the chaotic nature of a dynamic system and the strangeness of the attractor of a chaotic system. A dynamic system with a positive CD indicates chaotic behavior, and a larger CD indicates a more irregular attractor of a chaotic system. We calculate the CDs of chaotic maps with an embedding dimension of 2 using the method outlined in [45]. Two CDs can be calculated by taking each dimension output of a 2D chaotic map as the input of CD calculation. Table V lists the two CDs for our three new chaotic maps, as well as those of Bao, Huang, and Kong's 2D chaotic maps. It can be observed that the two CDs of our chaotic maps are larger than those of the comparative chaotic maps.

TABLE V
THE CDS OF 2D-FCCM, 2D-LCCM, AND 2D-SCCM AS WELL AS BAO'S, HUANG'S, AND KONG'S 2D CHAOTIC MAPS

	2D-F CCM	2D-L CCM	2D-S CCM	Bao's [41]	Huang's [42]	Kong's [43]
CD_1	1.9630	1.9677	1.9490	1.4293	1.5485	1.3748
CD_2	1.9612	1.9551	1.9033	1.6003	1.5309	1.6580

4) IE: IE is a commonly used measure for analyzing the randomness of a signal, and it can be used to evaluate the randomness of the state vectors generated by a chaotic system. The phase space of an nD chaotic system can be partitioned into I^n sub-phase spaces by equally dividing each dimension of the phase space into I intervals. If the probabilities of all state vectors falling into each sub-phase space are the same, then the IE achieves a theoretical maximum value of $IE_{\max} = n\log_2(I)$. The larger the IE, the more uniformly the state vector are distributed in the phase space.

The IE can be measured at a more granular level with a larger I, and Table VI lists the IEs of our three new chaotic maps and Bao's, Huang's, and Kong's 2D chaotic maps against different I, with the state vectors of length I^3 generated by each chaotic map being tested. It can be observed that the IEs of our chaotic maps are closer to $IE_{\max}$ and larger than those of the comparative chaotic maps for each I, implying that the state vectors of our chaotic maps have a more uniform distribution.

In summary, our three 2D chaotic maps share common advantages, such as unstable fixed points, the ability to delay chaos degradation, two positive LEs, uniformly distributed trajectories, and more. Consequently, they can all be regarded as exhibiting robust chaotic behaviors. The differences or potential disadvantages among them are attributed to the selection of the seed maps. The logistic map has the simplest complexity, while the fractional map boasts the highest complexity, resulting in different complexity levels for the three new 2D chaotic maps.

IV. NOISE-REDUCED OFDM-DCSK

This section details the proposed NR-OFDM-DCSK communication scheme and analyzes its theoretical BER over the AWGN channel.

A. NR-OFDM-DCSK Transmitter

Fig. 3 shows the transmitter structure of the NR-OFDM-DCSK communication scheme. Assuming $N-1$ information bits are transmitted at a time, the information bits first undergo binary phase shift keying (BPSK) modulation. Here, a binary 0 is modulated as a BPSK data -1 and a binary 1 is modulated as a BPSK data 1. The resulting $N-1$ BPSK data symbols are then simultaneously encoded using the same chaotic sequence via chaotic modulation after sequential-to-parallel (S/P) conversion. This results in $N-1$ information-bearing signals that are further processed through the scrambling module and the IFFT module, along with the reference signal (i.e., the used chaotic sequence). Finally, the obtained signals are transmitted after parallel-to-sequential (P/S) conversion. Our NR-OFDM-DCSK scheme can employ any chaotic systems. In different tests, the used chaotic systems can be different. When a chaotic system is employed in NR-OFDM-DCSK, all the used chaotic sequences are generated by the chaotic system.

1) Chaotic Modulation: Assume that the clock rate of NR-OFDM-DCSK is $1/T_c$, where T_c denotes the chip duration. The spreading factor β is defined as the number of chaotic samples used to carry each information bit, and $T_b = \beta T_c$ represents the bit duration. The system clock triggers the chaos generator to produce a new chaotic sample every PT_c ($P \geq 2$) time, resulting in β/P different chaotic samples being produced during T_b time. Moreover, each chaotic sample has P duplicates, which form a chaotic reference sequence of length β. On this basis, by exploiting the zero-mean nature of channel noise, the receiver can calculate the average value of every P samples to reduce the noise variance.

Precisely, during T_b time, the chaos generator produces β/P distinct chaotic samples, denoted as $\{\hat{c}_0, \hat{c}_1, \ldots, \hat{c}_{\beta/P-1}\}$, with each sample having P duplicates to form the chaotic reference sequence $\{c_k\}$ as

$$c_k = \hat{c}_{\lfloor k/P \rfloor}, \tag{20}$$

where $k \in \{0, 1, \ldots, \beta-1\}$ and $\lfloor\cdot\rfloor$ is the round down operator.

Let b_i be the i-th BPSK data symbol for $i \in \{1, 2, \ldots, N-1\}$, the chaotic modulation process is performed by multiplying b_i with each element of the chaotic reference sequence $\{c_k\}$. The resulting modulated symbols can be expressed as

$$d_{i,k} = b_i c_k, \tag{21}$$

where $i \in \{1, 2, \ldots, N-1\}$ and $k \in \{0, 1, \ldots, \beta-1\}$. Hence, each BPSK data symbol b_i is encoded as an information-bearing signal $\mathbf{d}_i = [d_{i,0}, d_{i,1}, \ldots, d_{i,\beta-1}]$. For simplicity, we denote $\mathbf{d}_0 = \{c_k\} = [c_0, c_1, \ldots, c_{\beta-1}]$ as the chaotic reference signal, which collaborates with the $N-1$ information-bearing signals to form a signal matrix $\mathbf{D} = [\mathbf{d}_0{}^T, \mathbf{d}_1{}^T, \ldots, \mathbf{d}_{N-1}{}^T]^T$, where $(\cdot)^T$ refers to the transpose operation. As the signal matrix $\mathbf{D}$ may contain consecutively repeated elements, it undergoes processing by a scrambling module to provide a lightweight security boost.

2) Scrambling: The scrambling is to disrupt the positions of the elements in the signal matrix $\mathbf{D}$, and we adopt the high-speed scrambling strategy introduced in [46] in our method. In the scrambling procedure, a scrambling pattern $\mathbf{S}$ is constructed to help scramble the signal matrix $\mathbf{D}$. Two chaotic sequences of length N and β are generated based on the user's secret key, and these two chaotic sequences are sorted to produce two index vectors $\mathbf{I}_1 \in \mathbb{N}^{1\times N}$ and $\mathbf{I}_2 \in \mathbb{N}^{1\times\beta}$. The key space is calculated as the product of the factorial of N and β ($N! \times \beta!$). In the scrambling process, each operation repeatedly employs these two identical chaotic sequences with fixed lengths N and β, respectively, which are different from the chaotic reference sequences used in modulation. The scrambling pattern $\mathbf{S} \in \mathbb{R}^{N\times\beta}$ can be obtained as [46]

$$\mathbf{S}(i,:) = \text{circshift}(\mathbf{I}_2, \mathbf{I}_1(i)), \tag{22}$$

where $\mathbf{S}(i,:)$ is the i-th row of $\mathbf{S}$ for $i \in \{1, 2, \ldots, N\}$, and circshift$(\mathbf{I}_2, \mathbf{I}_1(i))$ refers to the result of circularly shifting $\mathbf{I}_2$ by $\mathbf{I}_1(i)$ positions.

Using the scrambling pattern $\mathbf{S}$, we can scramble the signal matrix $\mathbf{D}$ to obtain $\mathbf{D}' \in \mathbb{N}^{N\times\beta}$ by moving the matrix elements to their new positions. Explicitly, for $x \in \{1, 2, \ldots, N\}$ and

TABLE VI
THE IES OF 2D-FCCM, 2D-LCCM, AND 2D-SCCM AS WELL AS BAO'S, HUANG'S, AND KONG'S 2D CHAOTIC MAPS AGAINST DIFFERENT I

I	8	10	12	14	16	18	20	22	24	26	28	30	32
$IE_{\max}$	6	6.6439	7.1699	7.6147	8	8.3399	8.6439	8.9189	9.1699	9.4009	9.6147	9.8138	10
2D-FCCM	5.9166	6.5609	7.1092	7.5683	7.9524	8.2996	8.6096	8.8893	9.1393	9.3742	9.5884	9.7886	9.9773
2D-LCCM	5.9248	6.5727	7.1178	7.5723	7.9614	8.3036	8.6096	8.8894	9.1423	9.3737	9.5889	9.7902	9.9782
2D-SCCM	5.9048	6.5657	7.1012	7.5602	7.9537	8.2971	8.6059	8.8798	9.1379	9.3741	9.5876	9.7906	9.9783
Bao's [41]	5.3015	6.0132	6.4779	6.8791	7.2826	7.6161	7.8655	8.1196	8.3750	8.5779	8.7449	8.9093	9.0666
Huang's [42]	5.6450	6.2916	6.7840	7.2219	7.5888	7.9092	8.2152	8.4713	8.7207	8.9478	9.1645	9.3510	9.5315
Kong's [43]	5.6912	6.2841	6.7600	7.1862	7.5186	7.8269	8.1288	8.3879	8.6249	8.8495	9.0475	9.2136	9.4031

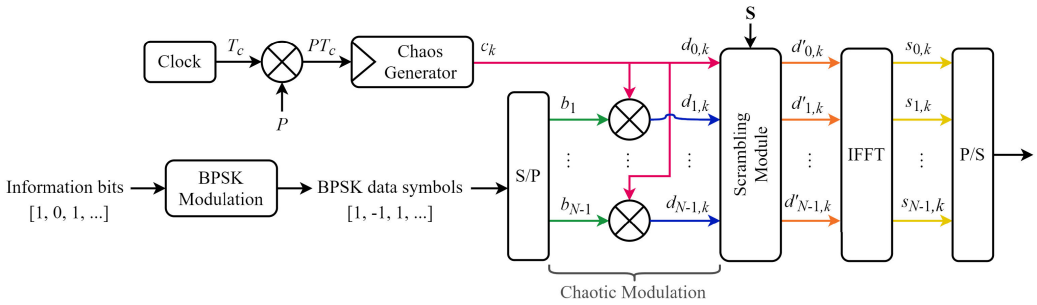

Fig. 3. The transmitter structure of our NR-OFDM-DCSK.

$y \in \{1, 2, \ldots, \beta\}$, the element at position $(x, \mathbf{S}(x, y))$ in $\mathbf{D}$ is relocated to position (x', y') in $\mathbf{D}'$, where x' and y' can be determined as follows [46]:

$$\begin{cases} x' = \big(x - \mathbf{S}(1, y) - 1 \mod N\big) + 1 \\ y' = \mathbf{S}(x', y). \end{cases} \tag{23}$$

The above process is reversible and the element at position $(x, \mathbf{S}(x, y))$ in $\mathbf{D}$ can be retrieved from the element located at position (x', y') in $\mathbf{D}'$. Once scrambling is completed, the scrambled signal matrix $\mathbf{D}'$ is transferred to the IFFT module.

3) IFFT: The IFFT operation is applied to each column of the scrambled signal matrix $\mathbf{D}'$. For $k \in \{0, 1, \ldots, \beta - 1\}$, the IFFT operation is performed on the k-th column of $\mathbf{D}'$ as

$$s_{n,k} = \frac{1}{\sqrt{N}} \sum_{i=0}^{N-1} d'_{i,k} e^{j\frac{2\pi i n}{N}}, \tag{24}$$

where $n \in \{0, 1, \ldots, N-1\}$, $d'_{i,k}$ denotes the element of $\mathbf{D}'$ at position (i, k), e is the Euler's number, and j is the imaginary unit. The IFFT operation on the k-th column of $\mathbf{D}'$ produces a vector $[s_{0,k}, s_{1,k}, \ldots, s_{N-1,k}]^T$, which is then converted by P/S conversion and transmitted to the communication channel.

B. NR-OFDM-DCSK Receiver

When receiving the transmission signal, the receiver is able to recover the transmitted information bits. The receiver structure of NR-OFDM-DCSK is illustrated in Fig. 4. As can be seen, after S/P conversion, the N received signals are processed by the FFT module and the descrambling module. Subsequently, each of the N signals is sent to an averaging filter, which is disciplined by the same parameter P as that used in the transmitter. The first filtered signal is explicitly stored in matrix $\mathbf{A}$, while the remaining $N-1$ filtered signals are stored in matrix $\mathbf{B}$. These two matrices are subsequently utilized in the chaotic demodulation process to recover the transmitted bits.

1) FFT: The FFT operation is performed on each column of the received signal matrix $\mathbf{R} \in \mathbb{C}^{N\times\beta}$. For $k \in \{0, 1, \ldots, \beta - 1\}$, the FFT operation is applied to the k-th column of $\mathbf{R}$ as

$$z'_{i,k} = \frac{1}{\sqrt{N}} \sum_{n=0}^{N-1} r_{n,k} e^{-j\frac{2\pi n i}{N}} = d'_{i,k} + \eta'_{i,k}, \tag{25}$$

where $i \in \{0, 1, \ldots, N-1\}$, $r_{n,k}$ denotes the element of $\mathbf{R}$ at position (n, k), and $\eta'_{i,k}$ refers to the channel noise. The signal $z'_{i,k}$ recovered by the FFT operation may be different from the original signal $d'_{i,k}$ when it is blurred by the channel noise during transmission.

2) Descrambling: Descrambling aims to restore each element's position in the signal matrix, which is the inverse process of scrambling. The receiver generates an identical scrambling pattern $\mathbf{S}$ with that in the transmitter to assist descramble. Denote $\mathbf{Z}' \in \mathbb{C}^{N\times\beta}$ as the signal matrix obtained from the FFT operation. In order to descramble $\mathbf{Z}'$ into the signal matrix $\mathbf{Z} \in \mathbb{C}^{N\times\beta}$, the element at position $(x, \mathbf{S}(x, y))$ in $\mathbf{Z}$ is retrieved from the element at position (x', y') in $\mathbf{Z}'$ using Eq. (23), in which $x \in \{1, 2, \ldots, N\}$ and $y \in \{1, 2, \ldots, \beta\}$. Without knowing the exact scrambling pattern $\mathbf{S}$, an eavesdropper cannot convert $\mathbf{Z}'$ to $\mathbf{Z}$. Subsequently, the descrambled signal matrix $\mathbf{Z}$ is subjected to the averaging filters for further processing.

3) Averaging Filtering: The averaging filtering operation is to mitigate the interference of noise on the transmitted signal. To accomplish this, N averaging filters concurrently process N rows of the signal matrix $\mathbf{Z}$. Specifically, an average value is calculated for every P samples in each row, where P is set the same as that in the transmitter. For $i \in \{0, 1, \ldots, N-1\}$ and $j \in \{0, 1, \ldots, \frac{\beta}{P} - 1\}$, the j-th output of the i-th averaging filter can be expressed as

$$g_{i,j} = \frac{1}{P} \sum_{k=jP}^{(j+1)P-1} z_{i,k} = \frac{1}{P} \sum_{k=jP}^{(j+1)P-1} (d_{i,k} + \eta_{i,k}), \tag{26}$$

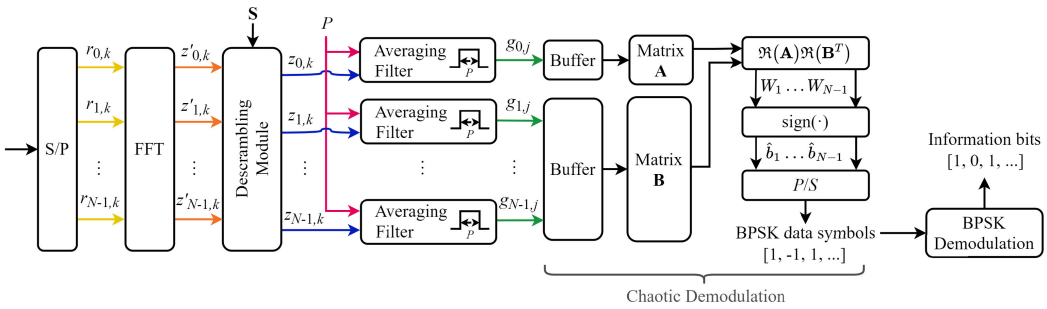

Fig. 4. The receiver structure of our NR-OFDM-DCSK.

where $z_{i,k} = d_{i,k} + \eta_{i,k}$ denotes the element of $\mathbf{Z}$ at position (i, k). Since the variance of the noise in $g_{i,j}$ is only $1/P$ of the noise's variance in $z_{i,k}$, the averaging filtering process can effectively reduce the noise on the transmitted signal.

The outputs of the first averaging filter and the rest $N-1$ filters are represented as matrices $\mathbf{A} \in \mathbb{C}^{1\times\frac{\beta}{P}}$ and $\mathbf{B} \in \mathbb{C}^{(N-1)\times\frac{\beta}{P}}$, respectively. Matrix $\mathbf{A}$ contains the chaotic reference signal, and matrix $\mathbf{B}$ contains the information-bearing signals. Afterwards, these two matrices are fed into the chaotic demodulation process to recover the information bits.

4) Chaotic Demodulation: The chaotic demodulation process is as follows:

$$[W_1, W_2, \dots, W_{N-1}] = \Re(\mathbf{A})\Re(\mathbf{B}^T), \tag{27}$$

where $\Re(\cdot)$ takes the real part of the complex signal, and W_i ($i \in \{1, 2, \dots, N-1\}$) is the product of the chaotic reference signal and the i-th information-bearing signal:

$$W_i = \sum_{j=0}^{\frac{\beta}{P}-1} \Re(g_{0,j})\Re(g_{i,j}). \tag{28}$$

Then, the estimated BPSK data can be determined from the sign of W_i as

$$\hat{b}_i = \text{sign}(W_i). \tag{29}$$

Finally, the information bits can be recovered from the BPSK data through BPSK demodulation, where the BPSK data -1 is demodulated as binary 0, and BPSK data 1 is demodulated to binary 1.

C. Theoretical BER Analysis

In this subsection, we delve into the theoretical BER of NR-OFDM-DCSK. Since AWGN is one of the most frequently occurring noises in the transmission channels, we analyze the theoretical BER of NR-OFDM-DCSK over the AWGN channel using the Gaussian approximation method [16]. Explicitly, the channel noise $\eta_{i,k} = \xi_{i,k} + j\zeta_{i,k}$ is the complex AWGN with zero-mean and power spectral density of N_0. In other words, the channel noise satisfies that $\text{E}\{\eta_{i,k}\} = \text{E}\{\xi_{i,k}\} = \text{E}\{\zeta_{i,k}\} = 0$ and $\text{E}\{|\eta_{i,k}|^2\} = 2\,\text{E}\{\xi_{i,k}{}^2\} = 2\,\text{E}\{\zeta_{i,k}{}^2\} = N_0$, where $\text{E}\{\cdot\}$ refers to the expectation notation.

To derive the theoretical BER for NR-OFDM-DCSK, we first reformulate the signal $g_{i,j}$ obtained from the last $N-1$ averaging filters based on Eqs. (26), (21), and (20) as below:

$$g_{i,j} = b_i\hat{c}_j + \frac{1}{P}\sum_{k=jP}^{(j+1)P-1} \eta_{i,k}, \tag{30}$$

where $i \in \{1, 2, \dots, N-1\}$, $j \in \{0, 1, \dots, \frac{\beta}{P}-1\}$, and $g_{i,j}$ essentially encompasses both the data sent from the transmitter and the noise signal acquired during the transmission process. As the output of the first averaging filter contains the chaotic reference signal without modulating any BPSK data, the expression for $g_{0,j}$ can be rewritten as

$$g_{0,j} = \hat{c}_j + \frac{1}{P}\sum_{k=jP}^{(j+1)P-1} \eta_{0,k}. \tag{31}$$

Subsequently, we can rewrite the chaotic demodulated result W_i ($i \in \{1, 2, \dots, N-1\}$) from Eqs. (28), (30), and (31) as

$$\begin{aligned} W_i &= \sum_{j=0}^{\frac{\beta}{P}-1} \Re\left(\hat{c}_j + \frac{1}{P}\sum_{k=jP}^{(j+1)P-1}\eta_{0,k}\right)\Re\left(b_i\hat{c}_j + \frac{1}{P}\sum_{k=jP}^{(j+1)P-1}\eta_{i,k}\right) \\ &= \sum_{j=0}^{\frac{\beta}{P}-1}\left(\hat{c}_j + \frac{1}{P}\sum_{k=jP}^{(j+1)P-1}\xi_{0,k}\right)\left(b_i\hat{c}_j + \frac{1}{P}\sum_{k=jP}^{(j+1)P-1}\xi_{i,k}\right) \\ &= \underbrace{\sum_{j=0}^{\frac{\beta}{P}-1} b_i\hat{c}_j^2}_{U_1} + \underbrace{\frac{1}{P^2}\sum_{j=0}^{\frac{\beta}{P}-1}\left(\left(\sum_{k=jP}^{(j+1)P-1}\xi_{0,k}\right)\left(\sum_{k=jP}^{(j+1)P-1}\xi_{i,k}\right)\right)}_{U_2} \\ &\quad + \underbrace{\frac{1}{P}\sum_{j=0}^{\frac{\beta}{P}-1}\left(\hat{c}_j\sum_{k=jP}^{(j+1)P-1}\xi_{i,k} + b_i\hat{c}_j\sum_{k=jP}^{(j+1)P-1}\xi_{0,k}\right)}_{U_3}, \end{aligned} \tag{32}$$

where part U_1 contains the transmitted BPSK data, and parts U_2 and U_3 contain the channel noise. Since U_1, U_2, and U_3 are statistically independent of each other, the expectation and variance of W_i can be obtained by separately adding up their expectations and variances as

$$\text{E}\{W_i|(b_i = \pm 1)\} = \sum_{l=1}^{3}\text{E}\{U_l|(b_i = \pm 1)\}, \tag{33a}$$

$$\text{Var}\{W_i|(b_i = \pm 1)\} = \sum_{l=1}^{3}\text{Var}\{U_l|(b_i = \pm 1)\}, \tag{33b}$$

where $\text{E}\{\cdot\}$ and $\text{Var}\{\cdot\}$ refer to the expectation and variance notations, respectively. As the chaotic samples are independent of the channel noise, which satisfies that $\text{E}\{\xi_{i,k}\} = 0$ and $\text{E}\{\xi_{i,k}{}^2\} = N_0/2$, the expectations and variances of U_1, U_2, and U_3 can be calculated as

$$\text{E}\{U_1|(b_i = +1)\} = -\,\text{E}\{U_1|(b_i = -1)\} = \frac{\beta}{P}\,\text{E}\{\hat{c}_j^2\}, \tag{34a}$$

$$\mathrm{E}\left\{U_2|(b_i=\pm1)\right\}=\mathrm{E}\left\{U_3|(b_i=\pm1)\right\}=0, \tag{34b}$$

$$\mathrm{Var}\left\{U_1|(b_i=\pm1)\right\}=\frac{\beta}{P}\mathrm{Var}\left\{\hat{c}_j^2\right\}, \tag{34c}$$

$$\mathrm{Var}\left\{U_2|(b_i=\pm1)\right\}=\frac{\beta N_0^2}{4P^3}, \tag{34d}$$

$$\mathrm{Var}\left\{U_3|(b_i=\pm1)\right\}=\frac{\beta N_0}{P^2}\mathrm{E}\left\{\hat{c}_j^2\right\}. \tag{34e}$$

Finally, based on the expectation and variance of W_i, we can derive the theoretical BER of NR-OFDM-DCSK as

$$\begin{aligned}
BER&=\frac{1}{2}\mathrm{erfc}\left(\sqrt{\Gamma/2}\right)\\
&=\frac{1}{2}\mathrm{erfc}\left[\left(\frac{2\,\mathrm{Var}\left\{W_i|(b_i=\pm1)\right\}}{\mathrm{E}\left\{W_i|(b_i=\pm1)\right\}^2}\right)^{-\frac{1}{2}}\right]\\
&=\frac{1}{2}\mathrm{erfc}\left[\left(\frac{2P\,\mathrm{Var}\left\{\hat{c}_j^2\right\}}{\beta\,\mathrm{E}\left\{\hat{c}_j^2\right\}^2}+\frac{N_0^2}{2P\beta\,\mathrm{E}\left\{\hat{c}_j^2\right\}^2}+\frac{2N_0}{\beta\,\mathrm{E}\left\{\hat{c}_j^2\right\}}\right)^{-\frac{1}{2}}\right]\\
&=\frac{1}{2}\mathrm{erfc}\left[\left(\frac{2P\,\mathrm{Var}\left\{\hat{c}_j^2\right\}}{\beta\,\mathrm{E}\left\{\hat{c}_j^2\right\}^2}+\frac{\beta N^2N_0^2}{2P(N-1)^2E_b^2}+\frac{2NN_0}{(N-1)E_b}\right)^{-\frac{1}{2}}\right],
\end{aligned} \tag{35}$$

where Γ is the signal-to-noise (SNR) expression [16] and it is shown as

$$\Gamma=\frac{\mathrm{E}\left\{W_i|(b_i=\pm1)\right\}^2}{\mathrm{Var}\left\{W_i|(b_i=\pm1)\right\}}, \tag{36}$$

The complementary error function, denoted as $\mathrm{erfc}(x)=\frac{2}{\sqrt{\pi}}\int_x^\infty e^{-t^2}\mathrm{d}t$ is a monotonically decreasing function, and $E_b=N\beta\,\mathrm{E}\{\hat{c}_j^2\}/(N-1)$ refers to the average bit energy. From Eq. (35), we can observe that for fixed P, β and N, the smaller variance $\mathrm{Var}\{\hat{c}_j^2\}$ and larger expectation $\mathrm{E}\{\hat{c}_j^2\}$ of the chaotic sequences $\hat{c}_j^2$ contribute to a decrease in BER. On one hand, our 2D chaotic maps can generate uniformly distributed trajectories, which can achieve relatively small variance $\mathrm{Var}\{\hat{c}_j^2\}$. On the other hand, our 2D chaotic map can output chaotic sequences with large expectation $\mathrm{E}\{\hat{c}_j^2\}$ by adjusting the modulus coefficient M of 2D-CCS in Eq. (1). As a result, our 2D chaotic maps can achieve small BER in secure communication. A detailed BER analysis in multipath fading is available in the Supplementary Material.

V. Performance Evaluation of NR-OFDM-DCSK

This section evaluates and discusses the performance of the NR-OFDM-DCSK communication scheme from four aspects: BER, energy efficiency, spectral efficiency, and complexity. Meanwhile, the proposed NR-OFDM-DCSK is compared with state-of-the-art communication schemes, including the OFDM-DCSK scheme [15], the FH-OFDM-DCSK scheme [16], and the OFDM-PC-CSK scheme [17]. Among them, OFDM-DCSK is the first scheme to introduce OFDM into DCSK and it suffers from a relatively high BER. FH-OFDM-DCSK improves the security of OFDM-DCSK but it does not enhance the BER performance in the AWGN channel. OFDM-PC-CSK has a high transmission efficiency with a high implementation complexity. Compared to these schemes, our NR-OFDM-DCSK scheme employs an averaging filtering technique that significantly reduces noise variance, thus enhancing BER performance effectively. Additionally, by using a scrambling module to randomize the elements of the transmission matrix, the security of our NR-OFDM-DCSK scheme is improved. Importantly, the NR-OFDM-DCSK scheme maintains lower complexity compared to OFDM-PC-DCSK [17], which will be evidenced in Table VII.

TABLE VII

The Energy Efficiency, Spectral Efficiency, and Complexity of NR-OFDM-DCSK, OFDM-DCSK, FH-OFDM-DCSK, and OFDM-PC-CSK

Schemes	Energy efficiency	Spectral efficiency	Complexity
NR-OFDM-DCSK	$(N-1)/N$	$(N-1)/(\beta BT_o)$	$O(N\beta\log_2 N)$
OFDM-DCSK [15]	$(N-1)/N$	$(N-1)/(\beta BT_o)$	$O(N\beta\log_2 N)$
FH-OFDM-DCSK [16]	$(N-1)/N$	$(N-1)/(\beta BT_o)$	$O(N\beta\log_2 N)$
OFDM-PC-CSK [17]	1	$N/(\beta BT_o)$	$O(N\beta\log_2 N)+O(N\beta\log_2\beta)+O(N\beta^2)$

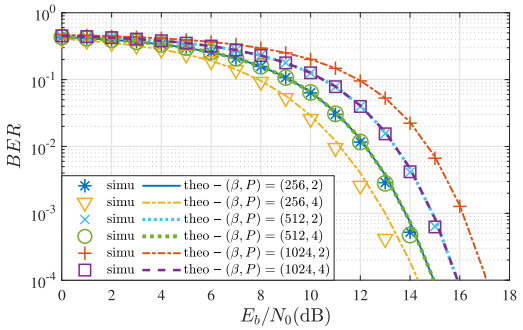

Fig. 5. The simulated and theoretical BERs of NR-OFDM-DCSK over the AWGN channel when $\beta\in\{256, 512, 1024\}$, $N=64$, and $P\in\{2, 4\}$.

A. BER Evaluation

1) BER of NR-OFDM-DCSK: We conduct two groups of experiments to verify the theoretical BER of the proposed NR-OFDM-DCSK. To generate chaos, we employ our new chaotic map, 2D-FCCM, defined by Eq. (14), as the chaos generator. The parameters p_1 and p_2 of 2D-FCCM are randomly selected within the range $[23, 122]$, and the first dimension output is used to carry the information bits. We then simulate the BER performance of NR-OFDM-DCSK over an AWGN channel, with the noise intensity quantified by the SNR ratio E_b/N_0.

The first group of experiments evaluates the BER performance of NR-OFDM-DCSK under different spreading factors $\beta\in\{256, 512, 1024\}$, with a fixed N of 64 and parameter $P\in\{2, 4\}$. As depicted in Fig. 5, the results reveal that the BER is lower when β is smaller, and our scheme can better suppress the noise to obtain a lower BER when P is larger. Moreover, it is evident that the theoretical BER is consistent with the simulated BER, with tiny difference caused by calculation error. Notably, the BER curves with identical β/P value overlap, such as the BER curve for parameters $(\beta, P)=(512, 2)$ overlapping with the BER curve for parameters $(\beta, P)=(1024, 4)$. This observation aligns with the theoretical BER formula for NR-OFDM-DCSK in Eq. (35), as reflected by both the β/P and P/β components.

The second group of experiments evaluates the BER performance of NR-OFDM-DCSK across varying numbers of subcarriers $N\in\{2, 64, 128\}$, with β fixed at 512 and parameter $P\in\{2, 4\}$. As illustrated in Fig. 6, the results indicate that as N increases, our scheme achieves a lower BER. However, when the ratio $N/(N-1)$ approaches 1, there is only a slight change in the BER, as evident from the results for $N\in$

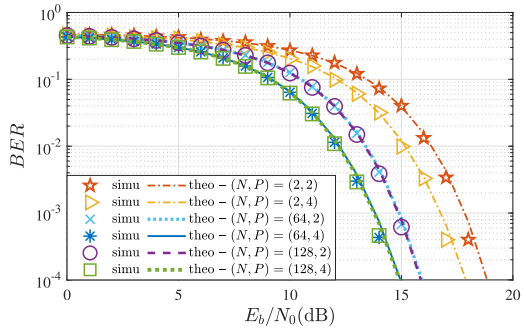

Fig. 6. The simulated and theoretical BERs of NR-OFDM-DCSK over the AWGN channel when $N \in \{2, 64, 128\}$, $\beta = 512$, and $P \in \{2, 4\}$.

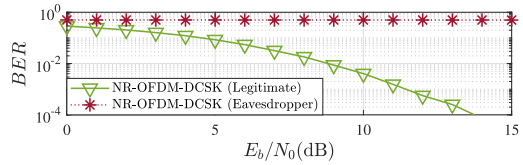

Fig. 7. The BERs of legitimate receiver and eavesdropper for NR-OFDM-DCSK when $\beta = 512$ and $N = P = 64$.

{64, 128}. This phenomenon also aligns with the theoretical BER formula of NR-OFDM-DCSK in Eq. (35), as indicated by the $N/(N-1)$ component. Moreover, the theoretical BER closely matches the simulated BER. Furthermore, the BER decreases with the increase of P, confirming the effectiveness of the averaging filter in reducing noise.

2) BER of Eavesdropper: In the structural design of NR-OFDM-DCSK, we provide a lightweight security boost for protecting the signal from transmission eavesdropping using a scrambling module. Without knowing the exact scrambling pattern $\mathbf{S}$, an eavesdropper cannot demodulate the transmitted information bits properly. Fig. 7 depicts the BERs of the legitimate receiver and eavesdropper for NR-OFDM-DCSK. As shown, the eavesdropper's BER remains at about 0.5, indicating that the information bits recovered by the eavesdropper are random sequences of 0s and 1s, which contain no useful information about the transmitted bits.

3) BER Comparison: To assess the effectiveness of our developed chaotic maps and the designed NR-OFDM-DCSK, we conduct three groups of experiments for BER comparison.

The first group of experiments compares the BER of NR-OFDM-DCSK when using different chaotic maps as the chaos generator. In particular, we use our new chaotic maps, namely 2D-FCCM, 2D-LCCM, and 2D-SCCM, along with the chaotic maps of Bao [41], Huang [42], Kong [43], 1D-Tent map [4] and 1D-Chebyshev map [4], as individual chaos generator for NR-OFDM-DCSK. To ensure stable and fair BER comparison, we conduct 100 experiments for each chaotic map and calculate the average BER. The parameters for each chaotic map in each experiment are chosen equidistantly from the parameter ranges used in the LE experiment in Section III-C.1. Additionally, the initial state of each chaotic map is randomly selected within $[0, 1) \times [0, 1)$. Moreover, since the outputs of different chaotic maps fall within varying ranges, we use the output of the first dimension of each chaotic map to carry the information bits after applying modulo one operation.

Fig. 8 illustrates the results of the first group of experiments. As shown, using our chaotic maps as the chaos generator results in significantly lower BERs for NR-OFDM-DCSK in comparison to other chaotic maps. In addition, we compare

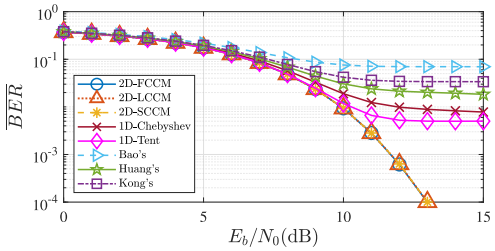

Fig. 8. BER comparison of NR-OFDM-DCSK over the AWGN channel using different chaotic maps as the chaos generator when $\beta = N = 64$ and $P = 2$.

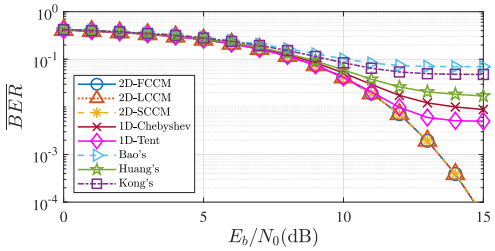

Fig. 9. BER comparison of NR-OFDM-DCSK over the combined AWGN and ARN channel using different chaotic maps as the chaos generator when $\beta = N = 64$ and $P = 2$.

the BER of NR-OFDM-DCSK using different chaotic maps as generators over the combined AWGN and ARN channel. As shown in Fig. 9, our chaotic maps also achieve lower BERs compared to other maps. These observations suggest that our chaotic maps are more suitable for secure communication applications, primarily due to their more continuous chaotic intervals. Furthermore, the BERs remain consistent when using our chaotic maps as the chaos generator. This is because three chaotic maps generated by the 2D-CCS exhibit uniformly distributed trajectories (as depicted in Figs. 2(a)-(c)) and similar chaotic complexities (as demonstrated in Tables V and VI). These imply the stability and reliability of our 2D-CCS framework in generating new chaotic maps well-suited for secure communication applications.

The second group of experiments involves comparing the BER performance among various communication schemes over the AWGN channel using our 2D-FCCM as the chaos generator, with the experimental results presented in Fig. 10. It can be observed that the BER of our NR-OFDM-DCSK outperforms other communication schemes, revealing its resilience to noise during transmission. In particular, when $E_b/N_0 \in \{0, 1, 2\}$ dB, the BER of OFDM-PC-CSK [17] is almost the same as that of our NR-OFDM-DCSK. However, as E_b/N_0 increases, our NR-OFDM-DCSK exhibits a substantially lower BER. Furthermore, we evaluate the BER performance of various communication schemes using our 2D-FCCM as the generator over the combined AWGN and ARN channel. Fig. 11 shows that our NR-OFDM-DCSK scheme achieves better BER performance than OFDM-DCSK and FH-OFDM-DCSK, and is similar to OFDM-PC-DCSK. However, it should be noted that OFDM-PC-DCSK incurs a higher computational cost, as detailed in Table VII.

The third group of experiments examines the BER performance of our proposed NR-OFDM-DCSK in other communication channels, including the flat fading channel and the multipath fading channel. These experiments also include a comparison among various communication schemes.

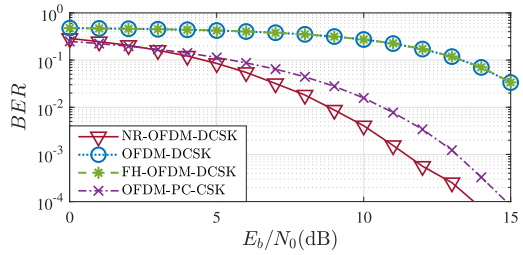

Fig. 10. BER comparison of NR-OFDM-DCSK over the AWGN channel with state-of-the-art communication schemes when $\beta = 512$ and $N = P = 64$.

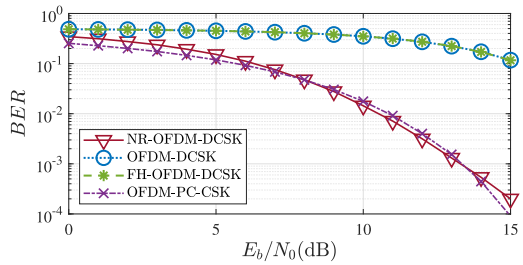

Fig. 11. BER comparison of NR-OFDM-DCSK over the combined AWGN and ARN channel with state-of-the-art communication schemes when $\beta = 1024$, $N = 64$ and $P = 128$.

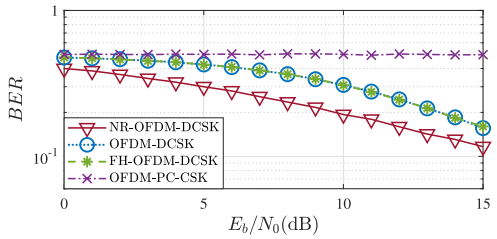

Fig. 12. BER comparison of NR-OFDM-DCSK over the flat fading channel with state-of-the-art communication schemes when $\beta = 512$ and $N = P = 64$.

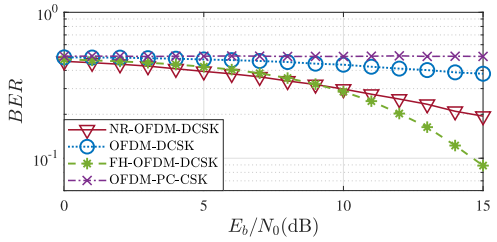

Fig. 13. BER comparison of NR-OFDM-DCSK over the multipath fading channel (with three paths) with state-of-the-art communication schemes when $\beta = 512$ and $N = P = 64$.

Fig. 12 depicts the BER comparison results for NR-OFDM-DCSK in the flat fading channel along with various communication schemes. It is evident that the BER of the proposed NR-OFDM-DCSK is consistently lower than that of other schemes, showing the advantage of our proposed scheme in the flat fading channel. Additionally, the results reveal that the designed averaging filters in the proposed scheme consistently effectively suppress noise in the flat fading channel.

Fig. 13 shows the BER comparison results for NR-OFDM-DCSK over the multipath fading channel along with various communication schemes. It can be observed that the BER of our proposed NR-OFDM-DCSK outperforms that of other schemes over the flat fading channel. For the multipath fading channel, our NR-OFDM-DCSK outperforms other schemes when $E_b/N_0 < 10$ dB. However, when $E_b/N_0 \geq 10$ dB, the BER of FH-OFDM-DCSK is the lowest. This can be attributed to the design of the frequency hopping module in the FH-OFDM-DCSK scheme, which is primarily designed to utilize the frequency diversity gain in the multipath fading channel. Moreover, the BER of OFDM-PC-CSK remains consistently at 0.5 in both the flat fading channel and multipath fading channel, indicating its inapplicability in such scenarios.

Combining the results of the second and third groups of experiments, it can be concluded that the proposed NR-OFDM-DCSK consistently outperforms other schemes in both the AWGN channel and the flat fading channel. In the multipath fading channel, it also exhibits superior performance compared to some other schemes.

Unlike the NR-DCSK scheme in [47], which modulates one bit at a time, our NR-OFDM-DCSK scheme enhances transmission efficiency by simultaneously modulating $N-1$ information bits simultaneously at one time. Additionally, our NR-OFDM-DCSK scheme significantly improves communication security through the adopted scrambling strategy and achieves a lower bit error rate by using the averaging filtering to reduce the noise variance, outperforming compared to the OFDM-DCSK scheme in [15]. Therefore, compared to previous schemes, our NR-OFDM-DCSK scheme has advantages in transmission efficiency, communication security, and BER.

B. Energy Efficiency, Spectral Efficiency, and Complexity

This subsection analyzes the energy efficiency, spectral efficiency and complexity of our NR-OFDM-DCSK and compares it with other schemes, and the results are shown in Table VII.

The energy efficiency is characterized by the data-energy-to-bit-energy-ratio (DBR). For our NR-OFDM-DCSK, $N-1$ BPSK data are modulated using the same chaotic reference sequence. As a result, the energy required for our scheme to transmit an information bit can be expressed as

$$E_b = E_{data} + E_{ref}/(N-1), \tag{37}$$

where E_{data} and E_{ref} denote the energy required for transmitting BPSK data and chaotic reference sequence, respectively, and $E_{data} = E_{ref} = \sum_{k=0}^{\beta-1} c_k^2$. Thus, the energy efficiency of our NR-OFDM-DCSK can be obtained by

$$DBR = E_{data}/E_b = (N-1)/N. \tag{38}$$

Similarly, the energy efficiency of OFDM-DCSK and FH-OFDM-DCSK is also $(N-1)/N$, whereas OFDM-PC-CSK has an energy efficiency of 1 as it does not transmit the reference signals. However, as N increases, the ratio $(N-1)/N$ approaches 1, and the energy efficiency of our NR-OFDM-DCSK can reach an impressive 99.22% when $N = 128$.

The spectral efficiency refers to the number of information bits transmitted per OFDM symbol. With $N-1$ information bits being transmitted during the same time period, the spectral efficiency of our NR-OFDM-DCSK can be expressed as (N-1)/(βBT_o), where B denotes the bandwidth occupied by an OFDM symbol, and T_o represents the duration of an OFDM symbol. Similarly, the spectral efficiency of OFDM-DCSK and FH-OFDM-DCSK is also $(N-1)/(\beta BT_o)$, whereas OFDM-PC-CSK achieves a spectral efficiency of $N/(\beta BT_o)$.

The complexity analysis of our NR-OFDM-DCSK is given as follows: (1) The complexities of the chaotic modulation and

demodulation process are $O(N\beta)$ and $O(N\beta/P)$, respectively; (2) The complexity of both the scrambling and descrambling process is $O(N\beta)$; (3) The complexity of both IFFT and FFT operations is $O(N\beta \log_2 N)$; (4) The complexity of averaging filtering is $O(N\beta)$. Therefore, the overall complexity of our NR-OFDM-DCSK is $O(N\beta \log_2 N)$, which is the same as that of OFDM-DCSK and FH-OFDM-DCSK. In contrast, OFDM-PC-CSK has the highest complexity since it contains some matrix operations.

As a result, our NR-OFDM-DCSK achieves a lower BER while maintaining the same efficiency and complexity as OFDM-DCSK and FH-OFDM-DCSK. However, OFDM-PC-CSK gains a slightly higher efficiency but at the cost of increased complexity.

VI. Conclusion

Existing chaos-based secure communication schemes have some defects in the used chaotic system and communication structure. This paper first introduces 2D-CCS, a general framework to construct new 2D chaotic maps with complex dynamics behavior by combining an existing 1D seed map with two linear expressions. It provides users great flexibility to choose seed maps and linear expressions to generate a large number of new 2D chaotic maps. We theoretically demonstrate the hyperchaotic behavior of 2D-CCS in the sense of LE and experimentally verify the complex dynamics behavior of three examples generated by 2D-CCS. Then, we design NR-OFDM-DCSK, a new communication scheme that can better carry information bits. We analyze the theoretical BER of NR-OFDM-DCSK over the AWGN channel and verify the consistency between the simulated BER and the theoretical BER. Experimental results show that our new chaotic maps are more suitable for communication applications than previous 2D chaotic maps, and our designed NR-OFDM-DCSK performs better than prior communication schemes in resisting noise. Future work will explore constructing robust chaotic systems by using distinct 1D chaotic maps or 2D chaotic maps as seed maps.

References

[1] D. Torrieri, *Principles of Spread-Spectrum Communication Systems*. Boston, MA, USA: Springer, 2005.

[2] E. N. Lorenz, "Deterministic nonperiodic flow," *J. Atmos. Sci.*, vol. 20, no. 2, pp. 130–141, Mar. 1963.

[3] M. Alawida, A. Samsudin, J. S. Teh, and R. S. Alkhawaldeh, "A new hybrid digital chaotic system with applications in image encryption," *Signal Process.*, vol. 160, pp. 45–58, Jul. 2019.

[4] I. Fister, M. Perc, S. M. Kamal, and I. Fister, "A review of chaos-based firefly algorithms: Perspectives and research challenges," *Appl. Math. Comput.*, vol. 252, pp. 155–165, Feb. 2015.

[5] J. C. L. Chan, T. H. Lee, and C. P. Tan, "Secure communication through a chaotic system and a sliding-mode observer," *IEEE Trans. Syst. Man, Cybern. Syst.*, vol. 52, no. 3, pp. 1869–1881, Mar. 2022.

[6] Y. Zhao, W. Zhang, H. Su, and J. Yang, "Observer-based synchronization of chaotic systems satisfying incremental quadratic constraints and its application in secure communication," *IEEE Trans. Syst. Man, Cybern. Syst.*, vol. 50, no. 12, pp. 5221–5232, Dec. 2020.

[7] M. Han, K. Zhong, T. Qiu, and B. Han, "Interval type-2 fuzzy neural networks for chaotic time series prediction: A concise overview," *IEEE Trans. Cybern.*, vol. 49, no. 7, pp. 2720–2731, Jul. 2019.

[8] C. Li, B. Feng, S. Li, J. Kurths, and G. Chen, "Dynamic analysis of digital chaotic maps via state-mapping networks," *IEEE Trans. Circuits Syst. I, Reg. Papers*, vol. 66, no. 6, pp. 2322–2335, Jun. 2019.

[9] C.-M. Lin, D.-H. Pham, and T.-T. Huynh, "Encryption and decryption of audio signal and image secure communications using chaotic system synchronization control by TSK fuzzy brain emotional learning controllers," *IEEE Trans. Cybern.*, vol. 52, no. 12, pp. 13684–13698, Dec. 2022.

[10] T. Yang, "A survey of chaotic secure communication systems," *Int. J. Comput. Cognit.*, vol. 2, no. 2, pp. 81–130, 2004.

[11] Y. Tao, Y. Fang, H. Ma, S. Mumtaz, and M. Guizani, "Multi-carrier DCSK with hybrid index modulation: A new perspective on frequency-index-aided chaotic communication," *IEEE Trans. Commun.*, vol. 70, no. 6, pp. 3760–3773, Jun. 2022.

[12] C. Bai, H.-P. Ren, M. S. Baptista, and C. Grebogi, "Digital underwater communication with chaos," *Commun. Nonlinear Sci. Numer. Simul.*, vol. 73, pp. 14–24, Jul. 2019.

[13] X. Cai, W. Xu, L. Wang, and G. Kaddoum, "Joint energy and correlation detection assisted non-coherent OFDM-DCSK system for underwater acoustic communications," *IEEE Trans. Commun.*, vol. 70, no. 6, pp. 3742–3759, Jun. 2022.

[14] G. Kolumbán, B. Vizvári, W. Schwarz, and A. Abel, "Differential chaos shift keying: A robust coding for chaos communication," in *Proc. Int. Workshop Nonl. Dyn. Electron. Syst.*, Seville, Spain, 1996, pp. 87–92.

[15] S. Li, Y. Zhao, and Z. Wu, "Design and analysis of an OFDM-based differential chaos shift keying communication system," *J. Commun.*, vol. 10, no. 3, pp. 199–205, 2015.

[16] Z. Liu, L. Zhang, Z. Wu, and J. Bian, "A secure and robust frequency and time diversity aided OFDM–DCSK modulation system not requiring channel state information," *IEEE Trans. Commun.*, vol. 68, no. 3, pp. 1684–1697, Mar. 2020.

[17] Z. Chen, L. Zhang, J. Zhang, Z. Wu, and D. Luobu, "An OFDM-based pre-coded chaos shift keying transceiver for reliable V2V transmission," *IEEE Trans. Veh. Technol.*, vol. 71, no. 6, pp. 6710–6715, Jun. 2022.

[18] Y. Ni, Z. Wang, Y. Fan, X. Huang, and H. Shen, "Memory-based event-triggered control for global synchronization of chaotic Lur'e systems and its application," *IEEE Trans. Syst. Man, Cybern. Syst.*, vol. 53, no. 3, pp. 1920–1931, Mar. 2023.

[19] L. Liu, M. Lei, and H. Bao, "Event-triggered quantized quasisynchronization of uncertain quaternion-valued chaotic neural networks with time-varying delay for image encryption," *IEEE Trans. Cybern.*, vol. 53, no. 5, pp. 3325–3336, May 2023.

[20] H. Bao, M. Hua, J. Ma, M. Chen, and B. Bao, "Offset-control plane coexisting behaviors in two-memristor-based Hopfield neural network," *IEEE Trans. Ind. Electron.*, vol. 70, no. 10, pp. 10526–10535, Oct. 2023.

[21] D. Li, S.-M. Lu, and L. Liu, "Adaptive NN cross backstepping control for nonlinear systems with partial time-varying state constraints and its applications to hyper-chaotic systems," *IEEE Trans. Syst. Man, Cybern. Syst.*, vol. 51, no. 5, pp. 2821–2832, May 2021.

[22] Y. Zhang, Z. Hua, H. Bao, H. Huang, and Y. Zhou, "An n-dimensional chaotic system generation method using parametric PASCAL matrix," *IEEE Trans. Ind. Informat.*, vol. 18, no. 12, pp. 8434–8444, Dec. 2022.

[23] H. Lin et al., "An extremely simple multiwing chaotic system: Dynamics analysis, encryption application, and hardware implementation," *IEEE Trans. Ind. Electron.*, vol. 68, no. 12, pp. 12708–12719, Dec. 2021.

[24] Q. Lai, Z. Wan, L. K. Kengne, P. D. Kamdem Kuate, and C. Chen, "Two-memristor-based chaotic system with infinite coexisting attractors," *IEEE Trans. Circuits Syst. II, Exp. Briefs*, vol. 68, no. 6, pp. 2197–2201, Jun. 2021.

[25] H. Chen, P. Chen, Y. Fang, F. Chen, and L. Kong, "Parallel differential chaotic shift keying with code index modulation for wireless communication," *IEEE Trans. Commun.*, vol. 70, no. 8, pp. 5113–5127, Aug. 2022.

[26] S. Chen, S. Yu, J. Lü, G. Chen, and J. He, "Design and FPGA-based realization of a chaotic secure video communication system," *IEEE Trans. Circuits Syst. Video Technol.*, vol. 28, no. 9, pp. 2359–2371, Sep. 2018.

[27] Z. Lin, S. Yu, J. Lü, S. Cai, and G. Chen, "Design and ARM-embedded implementation of a chaotic map-based real-time secure video communication system," *IEEE Trans. Circuits Syst. Video Technol.*, vol. 25, no. 7, pp. 1203–1216, Jul. 2015.

[28] X. Na, M. Zhang, W. Ren, and M. Han, "Multistep-ahead chaotic time series prediction based on hierarchical echo state network with augmented random features," *IEEE Trans. Cognit. Develop. Syst.*, vol. 15, no. 2, pp. 700–711, Jun. 2023.

[29] S. Feng, M. Han, J. Zhang, T. Qiu, and W. Ren, "Learning both dynamic-shared and dynamic-specific patterns for chaotic time-series prediction," *IEEE Trans. Cybern.*, vol. 52, no. 6, pp. 4115–4125, Jun. 2022.

[30] D. Li, M. Han, and J. Wang, "Chaotic time series prediction based on a novel robust echo state network," *IEEE Trans. Neural Netw. Learn. Syst.*, vol. 23, no. 5, pp. 787–799, May 2012.
[31] A. Pikovsky and A. Politi, *Lyapunov Exponents: A Tool to Explore Complex Dynamics*. Cambridge, U.K.: Cambridge Univ. Press, 2016.
[32] S. Sahoo and B. K. Roy, "Design of multi-wing chaotic systems with higher largest Lyapunov exponent," *Chaos, Solitons Fractals*, vol. 157, Apr. 2022, Art. no. 111926.
[33] U. Schwengelbeck and F. H. M. Faisal, "Definition of Lyapunov exponents and KS entropy in quantum dynamics," *Phys. Lett. A*, vol. 199, nos. 5–6, pp. 281–286, Apr. 1995.
[34] J. He, Y.-M. Liu, J.-K. Tian, and Z.-R. Ren, "New inclusion sets for singular values," *J. Inequal. Appl.*, vol. 2017, no. 1, pp. 1–8, Dec. 2017.
[35] T. Maunu, T. Zhang, and G. Lerman, "A well-tempered landscape for non-convex robust subspace recovery," *J. Mach. Learn. Res.*, vol. 20, no. 37, pp. 1–59, 2019.
[36] G. Chen and D. Lai, "Making a dynamical system chaotic: FeedBack control of Lyapunov exponents for discrete-time dynamical systems," *IEEE Trans. Circuits Syst. I, Fundam. Theory Appl.*, vol. 44, no. 3, pp. 250–253, Mar. 1997.
[37] J.-A. Lu, X. Wu, J. Lü, and L. Kang, "A new discrete chaotic system with rational fraction and its dynamical behaviors," *Chaos, Solitons Fractals*, vol. 22, no. 2, pp. 311–319, Oct. 2004.
[38] R. C. Hilborn, *Chaos and Nonlinear Dynamics: An Introduction for Scientists and Engineers*. London, U.K.: Oxford Univ. Press, 2000.
[39] Z. Hua, B. Zhou, and Y. Zhou, "Sine-transform-based chaotic system with FPGA implementation," *IEEE Trans. Ind. Electron.*, vol. 65, no. 3, pp. 2557–2566, Mar. 2018.
[40] P. L'Ecuyer and R. Simard, "TestU01: A c library for empirical testing of random number generators," *ACM Trans. Math. Softw.*, vol. 33, no. 4, pp. 1–40, Aug. 2007.
[41] B. Bao, K. Rong, H. Li, K. Li, Z. Hua, and X. Zhang, "Memristor-coupled logistic hyperchaotic map," *IEEE Trans. Circuits Syst. II, Exp. Briefs*, vol. 68, no. 8, pp. 2992–2996, Aug. 2021.
[42] H. Huang, S. Yang, and R. Ye, "Efficient symmetric image encryption by using a novel 2D chaotic system," *IET Image Process.*, vol. 14, no. 6, pp. 1157–1163, May 2020.
[43] S. Kong, C. Li, H. Jiang, Q. Lai, and X. Jiang, "A 2D hyperchaotic map with conditional symmetry and attractor growth," *Chaos, Interdiscipl. J. Nonlinear Sci.*, vol. 31, no. 4, Apr. 2021, Art. no. 043121.
[44] L. Lacasa and J. Gómez-Gardeñes, "Correlation dimension of complex networks," *Phys. Rev. Lett.*, vol. 110, no. 16, Apr. 2013, Art. no. 168703.
[45] P. Grassberger and I. Procaccia, "Characterization of strange attractors," *Phys. Rev. Lett.*, vol. 50, no. 5, pp. 346–349, Jan. 1983.
[46] Z. Hua, S. Yi, and Y. Zhou, "Medical image encryption using high-speed scrambling and pixel adaptive diffusion," *Signal Process.*, vol. 144, pp. 134–144, Mar. 2018.
[47] G. Kaddoum and E. Soujeri, "NR-DCSK: A noise reduction differential chaos shift keying system," *IEEE Trans. Circuits Syst. II, Exp. Briefs*, vol. 63, no. 7, pp. 648–652, Jul. 2016.

Zhongyun Hua (Senior Member, IEEE) received the B.S. degree in software engineering from Chongqing University, Chongqing, China, in 2011, and the M.S. and Ph.D. degrees in software engineering from the University of Macau, Macau, China, in 2013 and 2016, respectively.

He is currently a Professor with the School of Computer Science and Technology, Harbin Institute of Technology, Shenzhen, China. His works have appeared in prestigious venues, such as IEEE TRANSACTIONS ON INFORMATION FORENSICS AND SECURITY, IEEE TRANSACTIONS ON DEPENDABLE AND SECURE COMPUTING, IEEE TRANSACTIONS ON SIGNAL PROCESSING, IEEE TRANSACTIONS ON IMAGE PROCESSING, IEEE TRANSACTIONS ON CYBERNETICS, IEEE TRANSACTIONS ON INDUSTRIAL ELECTRONICS, CVPR, AAAI, and ACM MultiMedia. His current research interests include chaotic systems, multimedia security, and secure cloud computing. He has published more than 100 papers on the subject, receiving more than 7500 citations. He has been recognized as a Highly Cited Researcher 2023 and a Highly Cited Researcher 2022. He is also an Associate Editor of IEEE SIGNAL PROCESSING LETTERS and *International Journal of Bifurcation and Chaos in Applied Sciences and Engineering*.

Zihua Wu received the B.S. degree in software engineering from Jinan University, Guangzhou, China, in 2021. She is currently pursuing the M.S. degree in computer science and technology with Harbin Institute of Technology, Shenzhen, China. Her research interests include chaotic systems and secure communication.

Yinxing Zhang received the M.S. degree in fundamental mathematics from Guilin University of Electronic Technology, Guilin, China, in 2019, and the Ph.D. degree in computer science and technology from Harbin Institute of Technology, Shenzhen, China, in 2023.

He is currently a Lecturer with the Faculty of Information Engineering and Automation, Kunming University of Science and Technology, Kunming, China. His current research interests include chaotic systems and nonlinear system control.

Han Bao (Member, IEEE) received the B.S. degree in landscape design from Jiangxi University of Finance and Economics, Nanchang, China, in 2015, the M.S. degree in art and design from Changzhou University, Changzhou, China, in 2018, and the Ph.D. degree in nonlinear system analysis and measurement technology from Nanjing University of Aeronautics and Astronautics, China, in 2022.

In 2019, he visited the Computer Science Department, The University of Auckland, New Zealand. He is currently an Associate Professor with the School of Microelectronics and Control Engineering, Changzhou University. His research interests include memristive neuromorphic circuits, nonlinear circuits and systems, and artificial intelligence.

Yicong Zhou (Senior Member, IEEE) received the B.S. degree in electrical engineering from Hunan University, Changsha, China, in 1992, and the M.S. and Ph.D. degrees in electrical engineering from Tufts University, Medford, MA, USA, in 2008 and 2010, respectively.

He is currently a Professor with the Department of Computer and Information Science, University of Macau, Macau, China. His research interests include image processing, computer vision, machine learning, and multimedia security.

Dr. Zhou is a fellow of the Society of Photo-Optical Instrumentation Engineers (SPIE) and was recognized as one of the World's Top 2% Scientists and one of the Highly Cited Researchers in 2020 and 2021. He received the Third Price of Macao Natural Science Award as a Sole Winner in 2020 and a co-recipient in 2014. He has been the leading Co-Chair of the Technical Committee on Cognitive Computing in the IEEE Systems, Man, and Cybernetics Society since 2015. He serves as an Associate Editor for IEEE TRANSACTIONS ON NEURAL NETWORKS AND LEARNING SYSTEMS, IEEE TRANSACTIONS ON CIRCUITS AND SYSTEMS FOR VIDEO TECHNOLOGY, and IEEE TRANSACTIONS ON GEOSCIENCE AND REMOTE SENSING.